Journal of Materials Processing Technology 232 (2016) 1–8

Contents lists available at ScienceDirect

Journal of Materials Processing Technology

journal homepage: www.elsevier.com/locate/jmatprotec

The effect of laser remelting on the surface chemistry of Ti6al4V components fabricated by selective laser melting

Jayasheelan Vaithilingam [a,*], Ruth D. Goodridge [a], Richard J.M. Hague [a], Steven D.R. Christie [b], Steve Edmondson [c]

[a] Additive Manufacturing and 3D Printing Research Group, School of Engineering The University of Nottingham, Nottingham, NG7 2RD, UK
[b] Department of Chemistry, Loughborough University, Loughborough, LE11 3TU, UK
[c] School of Materials, The University of Manchester, Manchester, M13 9PL, UK

ARTICLE INFO

Article history:
Received 20 May 2015
Received in revised form
21 December 2015
Accepted 21 January 2016
Available online 24 January 2016

Keywords:
Additive manufacturing
3D-printing
Selective laser melting
Ti6Al4V
Surface remelting
Surface chemistry

ABSTRACT

Surface remelting/skin scanning of components is generally performed during the selective laser melting (SLM) process to improve the surface quality of a part. However, the chemical effects of surface remelting are not well understood. In this study, cuboidal parts fabricated with and without laser remelting were characterised using scanning electron microscopy (SEM), surface profilometry and X-ray photoelectron spectrophotometry (XPS). The SEM images showed a low-amplitude undulating pattern was observed on both surfaces. The surface chemistries of the surface remelted/skin scanned (SK) and non-surface remelted/non-skin scanned (NSK) samples were observed to significantly differ in their elemental composition. The thickness of the surface oxide layer of the SK surface was double that of the NSK surface. Also, the contribution of the major alloying elements, including titanium and aluminium, on the surface oxide layer varied for both NSK and SK surfaces. The surface chemistry of the NSK and SK surface was significantly different to a conventionally forged (CF) Ti6Al4V surface. The rate of decrease of oxide with depth was in the order of CF > NSK > SK. Although surface remelting is useful in rendering improved surface quality, its impact on surface chemistry should be carefully considered.

1. Introduction

Selective laser melting (SLM) is a metal-based additive manufacturing (AM) technique capable of fabricating parts directly from three dimensional (3D) computer models. Due to its increased geometrical freedom, the use of SLM to fabricate customised designs with complex internal and external structures is explored widely for various applications including in the automotive, aerospace and biomedical industries (Gibson et al., 2010). In addition, SLM is widely regarded as an enabler of direct manufacture of end-use parts.

Although SLM has numerous advantages over conventional manufacturing such as moulding, die casting etc., the surface quality of a part produced by SLM is generally inferior. Vaithilingam et al. (2015) observed a surface roughness (Ra) of 17.6 μm ± 2 μm for Ti6Al4V components fabricated using Renishaw's AM 250 SLM machine. Alrbaey et al. (2014) reported a Ra value of 12.4 μm ± 3 μm for stainless steel components fabricated by employing the Renishaw's SLM 125 machine. Meier and Haberland (2008) witnessed the surface quality of vertical walls to be lower than the horizontal surfaces due to partially melted particles. Thus, in order to improve the surface quality of a SLM fabricated part, various post-processing techniques including sand blasting, machining, etching, electropolishing and plasma spraying, are employed. However, it is time consuming and not always possible to use these techniques on certain complex parts. Thus, the opportunity to improve the surface quality of a part during the SLM process is favoured in order to enable the direct manufacture of a greater range of parts without the need for post-processing.

Optimisation of SLM process parameters (including hatch spacing, hatch distance, feed powder particle size) performed by Yadroitsev and Smurov (2011) was observed to be useful in improving surface quality to some degree; however, it did not render the desired surface finish for a large number of applications. Kruth et al. (2010) proposed laser surface remelting as a potential solution to improve surface quality during the SLM process. In this approach, the top/final surface of the part is remelted after the actual laser scanning which melts and fuses the material. By surface remelting, a significant reduction in the surface roughness (Ra) pattern from 12 μm to 1.5 μm was observed. Yasa and Kruth (2011) have also

* Corresponding author. Fax: +44 115 95 13948.
E-mail address: Jayasheelan.Vaithilingam@nottingham.ac.uk (J. Vaithilingam).

http://dx.doi.org/10.1016/j.jmatprotec.2016.01.022

observed remelting the top layer to yield an improved surface finish. Alrbaey et al. (2014) indicated that on laser remelting of 316L stainless steel, the surface finish of SLM fabricated components can be improved by 80% than that of the initially fabricated surface (without surface remelting). Currently surface remelting, also called *skin scanning,* is performed by many SLM users to enhance the surface quality of SLM parts.

Surface remelting of the uppermost layer may be advantageous from a surface quality/finish point of view. However, surface remelting may affect the surface chemistry of the part. When a layer of a part fabricated by SLM is exposed to surface remelting, this will significantly increase the temperature and re-melt the previously-scanned layer. Since SLM is characterised by a rapid melting and cooling process, chemical transformations are possible depending on the elements in the material, melting and cooling rate and build atmosphere. Such chemical transformations may potentially deteriorate the surface properties, including surface chemistry, of the part. For example, when Kruth et al. (2010) processed Ti6Al4V by SLM, due to higher energy input and rapid solidification, formation of dark zones were witnessed. These dark zones were observed to contain a high concentration of aluminium due to segregation.

For commercially pure titanium, there may not be this segregation effect since it does not contain other metals; however, alteration in the surface oxide thickness is possible due to the rapid heating and cooling cycles in the presence of oxygen. Ti6Al4V is preferred in various applications because it displays enhanced corrosion resistance due to the presence of a stable TiO_2 film at high concentration on the surface (Warnke et al., 2009). Segregation of aluminium might alter this oxide layer and reduce the concentration of titanium oxide. This may potentially reduce the corrosion resistance and lead to failure of the part.

There is no previous literature that has investigated the effect of laser remelting of SLM produced parts on its surface chemistry (in the first few atomic layers) in detail. Hence in this study, Ti6Al4V, a grade 5 titanium alloy, was used to fabricate parts with skin scan (SK) and without skin scan (NSK) by SLM and the surface chemistry of these parts was examined.

2. Materials and methods

2.1. Material

Plasma atomised Ti6Al4V powder was purchased from LPW Technology Ltd., UK. The particle size (Dv 50, the particle size below which 50% of the sample volume is represented) was 33.2 μm. A conventionally forged (CF) Ti6Al4V plate was purchased from TIMET UK Ltd., UK. The CF sample was used to study the differences in surface chemistry between SLM fabricated NSK and SK surfaces and the CF surface. Solvents including dichloromethane, methanol and ethanol were purchased from Sigma Aldrich, UK.

2.2. Methods

2.2.1. CAD model

Cuboidal parts with the dimensions of 10 mm × 10 mm × 5 mm were designed using Magics 14.1 (Materialise) software and saved in a STL file format. The STL file was then sliced with 50 μm layer thickness. This design was then replicated to fabricate the required number of samples.

2.2.2. Selective laser melting

The cubical parts were fabricated in a Renishaw AM 250 machine using Ti6Al4V powder. The AM 250 machine was equipped with a fibre modulated pulse laser with a maximum power of 200 W and wavelength (λ) of 1070 nm. The AM 250 machine consisted of a hopper, a wiper, an elevator that lowered the substrate to adjust the layer thickness and a lens that focused the laser (200 W maximum) to the build area (250 × 250 × 300 mm). Before SLM, the Ti6Al4V powder from which the part was to be fabricated was spread over the build platform from the hopper to a pre-defined layer thickness. After the layer had been spread, the laser beam scanned and fused the powder in the areas specified by the layer of the CAD file.

Table 1
Process parameters used fabricate non-skin scanned (NSK) and skin scanned (SK) Ti6Al4V surfaces in an SLM.

Standard	No skin scan (NSK)	Skin scan (SK)
Laser power P (W)	200	200
Hatch spacing (μm)	100	100
Point distance (μm)	50	50
Exposure time (μs)	220	220
Layer thickness (μm)	50	50
Scan strategy	Meander	Meander
Build plate temperature (°C)	80	80
No. of shell scan	1	2

Previously optimised SLM process parameters used for the study are tabulated in Table 1. As can be observed from the table, the only change in the process parameters between the NSK and SK was the skin scanning. A multi-directional meander scan strategy was used where the laser scan direction was rotated by 67° for each layer to reduce the residual stress. The components were built on a Ti6Al4V metal substrate preheated to 80 °C. The build chamber was filled with argon gas to maintain an inert atmosphere. The temperature of the build chamber during the process was measured to be 34–36 °C.

2.2.3. Sample preparation

The SLM fabricated samples were removed from the substrate and sonicated in dichloromethane (DCM), methanol, ethanol and deionised water for 10 min each to remove loosely bound Ti6Al4V particles and other surface contaminants. The substrates were then dried using compressed air before surface characterisation. The CF sample was polished using a series of silicon carbide grits and diamond pastes. The polished samples were cleaned as above before surface characterisation.

2.2.4. Surface characterisation

Surface morphology

A Phillips (PW 6800/70) scanning electron microscope (SEM) was used to obtain the surface morphology of SLM fabricated Ti6Al4V surfaces. SEM was operated at a power of 20 kV and images were obtained at various magnifications.

Surface roughness

Surface roughness patterns of the NSK and SK surfaces were obtained using an Alicona InfiniteFocus® optical 3D measurement device. The Ra value was calculated by averaging the values obtained for five different samples from 175 μm^2 of each sample. The reported values are the mean ± standard error of the mean.

Surface chemistry

A Thermo Scientific K-Alpha X-ray photoelectron spectroscopy (XPS) was used to obtain the surface chemistry of the Ti6Al4V surface. XPS probing of the Ti6Al4V metal surface was performed on a random selection of areas which were considered to have acceptable flatness. Depth profiling was performed to study the elemental distribution and the oxide layer thickness of the SLM fabricated Ti6Al4V surface. Depth profiles were obtained by sputtering the specimen at a rate of approximately 1.35 Angstrom/sec (for titanium) using an argon ion gun. The probing spot size used to obtain the measurement was 400 μm. Aluminium (Al) Kα monochromated radiation at 1486.6 eV was used and photoelectrons were collected at a take-off angle of 90°. Survey spectra were collected at a pass energy of 100 eV in a constant energy analyser mode. High resolution spectra were obtained at a pass energy of 20 eV. Peak

Table 2
Relative atomic percentage of elements obtained using an X-ray photoelectron spectroscopy. Instrumental error due to calibration was approximated to ±10%.

Sample type	Relative atomic percentage of detected elements					
	Al 2p	*C 1s*	*N 1s*	*O 1s*	*Ti 2p*	*V 2p*
No skin scan (NSK)	9.3 ± 0.6	27.3 ± 0.9	6.1 ± 0.1	45.6 ± 0.9	11.5 ± 0.4	0.3 ± 0.1
Skin scan (SK)	12.2 ± 0.6	26.5 ± 0.7	4.1 ± 0.4	46.5 ± 0.5	10.5 ± 0.5	0.3 ± 0.1
Conventional sample (CS)	3.0 ± 0.9	32.57 ± 2.3	1.77 ± 0.3	49.17 ± 1.4	13.16 ± 1.2	0.3 ± 0.2

deconvolution was performed using Gaussian–Lorentzian curves and was used to investigate the different chemical states. A built-in Thermo Avantage data system was used for data acquisition and processing. The National Institute of Standards and Technology (NIST) database and previously reported literature by Aronsson et al., 1997; Ask et al., 1989; Dementjev et al., 2000; Variola et al., 2008 were used to identify the unknown spectral lines. Statistical analysis of the XPS results was performed by analysing three areas of each NSK, SK and CF sample. The equipment error due to calibration for this study was ± 10% in addition to the reported mean ± standard error of the mean.

3. Results

3.1. Surface morphology

Fig. 1 show the surface morphologies (top surface) of a NSK and a SK part fabricated using the SLM process. Both the NSK and SK surfaces showed some particles partially melted to the surface; however, the number of particles partially melted to the SK surface was fewer than the NSK surface. A possible reason for these partially melted/attached particles may have been due to the blowing of particles into the build area by the gassing unit of the SLM machine before the top layer had fully solidified. The surface morphology clearly showed the laser scan track during the SLM process.

An elevated ridge of the solidified material on the edges of both the NSK and SK parts can be observed from Fig. 2. This was mainly because the remelted material is partially pushed by the laser beam to the contour of the part. Both the NSK and SK surfaces were observed to be rough (Ra = 3.4 μm ± 0.2 μm for NSK and Ra = 2.2 μm ± 0.16 μm for SK) due to the presence of partially melted particles and laser scan tracks.

3.2. Surface chemistry

Table 2 exhibits the relative atomic percentage of elements obtained from the NSK and SK sample surfaces using XPS. The surfaces of the NSK, SK and CF samples were witnessed to have higher carbon and nitrogen concentration than expected, possibly due to surface contaminants as witnessed by Vaithilingam et al. (2014). If the surface is contaminated, direct interpretation of the atomic percentage obtained using XPS will lead to false conclusion. Hence the ratio of the underlying base elements was used to obtain the actual surface elemental composition. Ti:Al ratio for the NSK sample was observed to be 1.2 whereas for the SK sample the ratio was 0.9. This change in the surface elemental composition was significant and clearly demonstrated an increase in the surface aluminium concentration on skin scanning. However for the CF sample, the Ti:Al ratio was 4.4 and is significantly higher than the Ti:Al ratio observed for NSK and SK surfaces. This clearly shows that SLM of Ti6Al4V has a significant impact on the surface chemical composition. Although Ti6Al4V has 4% vanadium in the bulk material composition, a significantly lower concentration of approximately 0.3 ± 0.1% vanadium was observed for all NSK, SK and CF surfaces on their outermost layer. However, the ratio of Ti:V (38 for NSK and 35 for SK) showed a small increase in the surface vanadium concentration after skin scanning.

To investigate the elemental distribution in detail, depth profiling of both NSK and SK surfaces was performed. Figs. 3 and 4 show the evolution of the constituent elements on the NSK and SK surfaces including carbon, nitrogen, oxygen, titanium, aluminium and vanadium over the first few atomic layers (56 nm). On deconvoluting the C 1s region (Fig. 3) of the NSK and SK surfaces, peaks were observed at 285 ± 0.2 eV, 286.7 ± 0.1 eV and 288.2 ± 0.2 eV. These peaks were attributed to C—C, C—O/C—N and C═O respectively (Variola et al., 2008). For both the NSK and SK surfaces, carbon observed on their outermost layer vanished on etching the surface for ~4 nm. This clearly showed that the carbon was mainly due to the contamination of the surface. The peak observed at approximately 282 eV for both the NSK and SK sample after etching their outermost layer was attributed to metal carbide (Ask et al., 1989).

The deconvoluted N 1s region exhibited the possibility for peaks at 396.5 ± 0.2 eV and 400.2 ± 0.3 eV which corresponds to inorganically (metal–nitrogen) and organically (C—N) bound nitrogen to the surface (Dementjev et al., 2000). On etching the surface for approximately 4 nm, the organically bound nitrogen disappeared. This reveals that this nitrogen is possibly from nitrogen containing carbon contaminants (natural proteins/oils in the atmosphere). The peak at 396.5 ± 0.3 eV which was primarily due to metal nitride was observed until the final sampling depth (approximately 56 nm).

The deconvoluted O 1s peak exhibited the possibility of the presence of TiO_x at 530.4 ± 0.1 eV, C—O 531.6 ± 0.2 eV and adsorbed water molecules at 532.4 ± 0.2 eV for both NSK and SK samples (Variola et al., 2008). On deconvoluting the Ti 2p region (Fig. 4), the presence of TiO_2 (458.9 ± 0.3 eV), Ti_2O_3 (456.6 ± 0.2), TiO (455.5 ± 0.1 eV) and the underlying metal (454.2 ± 0.3 eV) was witnessed. The deconvoluted Al 2p region showed the presence of aluminium in its oxide (74.4 ± 0.2 eV) and metallic form (72.1 ± 0.1 eV). The surface vanadium concentration was too low for XPS to detect; however, the observed peak corresponded to vanadium in its oxide form (516. 2 eV) i.e. V_2O_5 (Biesinger et al., 2010).

Depth profiling results (Fig. 4) demonstrated a clear transition of metal oxides of titanium, aluminium and vanadium to their corresponding pure metal for both NSK and SK surfaces. However, this transformation of oxides to pure metal was more gradual for SK compared to NSK (circled in Fig. 4 with dotted lines). This slow transition may be due to the formation of a thick surface oxide film on the SK surface. Fig. 5a and b represent the evolution of elements on depth profiling of NSK and SK Ti6Al4V samples using XPS. As mentioned earlier, the increase in the titanium concentration and decrease in the oxygen concentration for the SK surface was more gradual than for the NSK surface. In addition to this, the concentration of aluminium on the SK surface was observed to be significantly increased compared to the NSK surface. This increase in aluminium concentration can be attributed to its increase in the surface elemental composition.

The surface oxide film thicknesses of the NSK and SK surfaces were measured by two different methods and are reported in Fig. 5. In the first, the thickness was measured based on the point at which the concentration of the major alloying element Ti was equal to that of oxygen. In the second method, the thickness was taken as the point at which the maximum observed concentration of oxygen had reduced to half. Using the initial method, the NSK sample showed

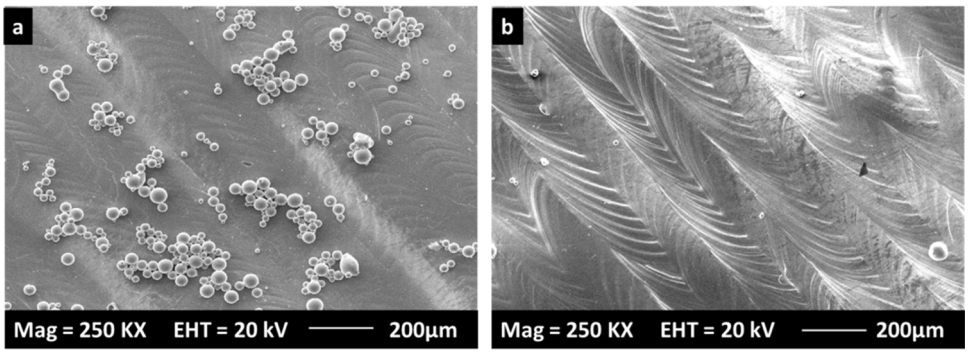

Fig. 1. Surface morphology of non-skin scanned and skin scanned Ti6Al4V SLM surfaces showing the laser scan tracks. The working distance for (a) (27.7 mm) and (b) (27.9 mm) are slightly different due to the presence of Ti6Al4V particles.

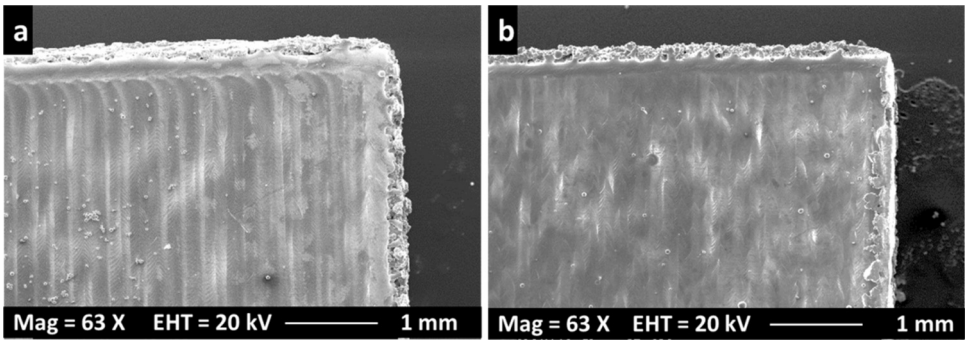

Fig. 2. Surface morphology of a non-skin scanned (a) and skin scanned (b) Ti6Al4V part fabricated by SLM.

a thickness of approximately 7 nm whereas the SK part showed approximately 14 nm which was nearly double that of the NSK's oxide layer thickness. In method 2, for NSK, the initially observed maximum detected O concentration of 46% reduced to 23% at nearly 35 nm; whereas for the SK surface, the initial maximum O concentration of nearly 47% did not reduce to half until the sampling depth of 56 nm. Both methods revealed that the thickness of the surface oxide film was higher for the SK surface than the NSK surface.

The ratio of the metals to oxide (Ti + Al + V:O) of the NSK, SK and CF samples as a function of depth were compared to study the spatial transition between surface metal oxide and the bulk, and are plotted in Fig. 6. Although the surfaces (depth = 0) are very similar, clear and significant differences in the depth distribution of the oxides for the SLM fabricated NSK, SK surfaces and the CF sample were observed. The rate of decrease of oxide with depth was in the order of CF > NSK > SK. The possible reasons for the varied elemental distribution and surface oxide transition are discussed below.

4. Discussion

In this study, both the NSK and SK parts fabricated using the AM 250 were observed to be slightly rough due to the presence of partially melted particles. In agreement with Meier and Haberland (2008), this study also observed the surface quality of the vertical surfaces to be inferior compared to the top/horizontal surface. Particles were also observed on the vertical sides of the cuboidal samples (other than top surface) and were primarily due to the partial melting of particles to the build surface. However, the partially sintered particles observed on the top horizontal surface might be due to the blowing of metal particles into the laser melted zones by the argon gas flow in the build chamber. Particles may also flow from the powder bed to the build due to small vibrations/movement of the wiper that may occur during the process.

Apart from the partially melted particles, laser scan tracks were clearly visible in the surface morphology of the NSK and especially on the SK surfaces. Since the SK surfaces were scanned by the laser twice, the scan tracks were more clearly visible. The SK surface was relatively smooth compared to the NSK surface since uneven morphologies were smoothened due to laser remelting. However, it should also be noted that as a result of remelting, laser scan tracks were witnessed and this might potentially affect the surface profile. The obtained Ra value for SK surfaces in this study was comparable to the previously reported value of 1.5 µm for SK surface by Yasa and Kruth (2011). The reduction in the Ra value from 3.4 µm ± 0.2 µm to 2.2 µm ± 0.16 after remelting clearly shows an improvement in the surface quality. Thus the surface remelting is useful to enhance the surface quality.

Kruth et al. (2010) suggested the use of skin scanning (remelting) for an improved surface quality and mechanical properties. However, the surface chemistry of such skin scanned surfaces has not been discussed. This study witnessed a high concentration of aluminium in the SK surface compared to the NSK surface. Although the Ti6Al4V alloy has only 6% Al in the bulk, more than 10% was observed on the NSK surface and over 15% of Al on the SK surface. However, only 3% was witnessed for the CF surface. One of the possible reasons for the increase in the concentration of Al on the NSK and SK surface than the actual alloy concentration may possibly due to rapid melting and solidification during the SLM process (Kruth et al., 2010).

The superior mechanical property of the titanium alloys compared to the commercially pure titanium (cpTi) is due to its phase composition. At room temperature, the cpTi is composed of a hexagonal closed-pack (hcp) α phase. However, when the temperature is raised to 882 °C (β transition temperature), the cpTi will undergo an allotropic transformation from hcp α phase to a body centred cubic (bcc) β phase (Kruth et al., 2010). Hence to alter the α-β transition temperature and obtain α+β alloy of titanium, alloy-

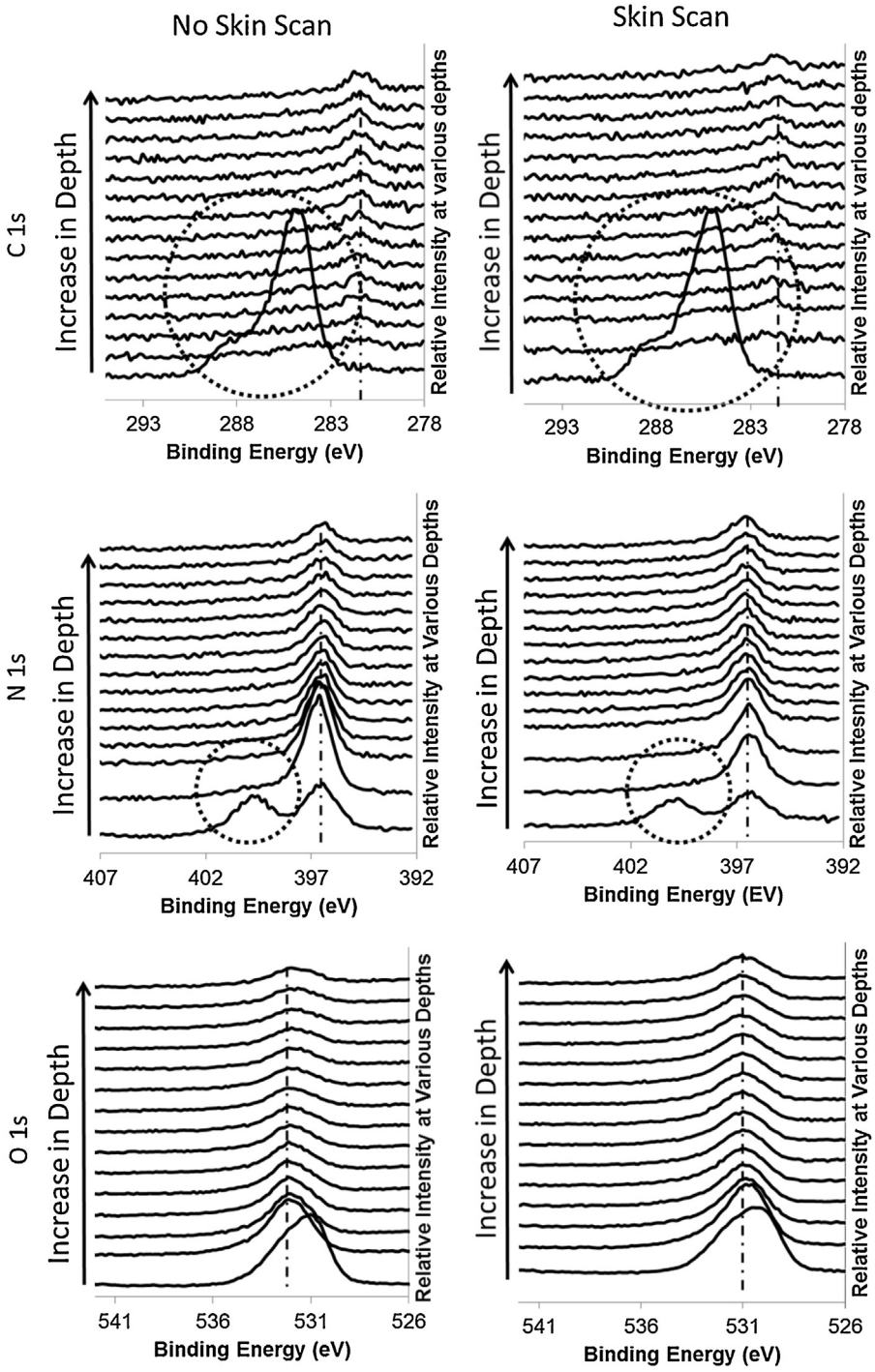

Fig. 3. XPS spectra of C 1s, N 1s and O 1s regions for the non-skin scanned (NSK) and skin scanned (SK) Ti6Al4V surfaces fabricated by SLM. The dotted circles show the presence of carbon and nitrogen from contamination and their disappearance after etching the surface.

ing elements such as aluminium, tin, vanadium and molybdenum are dissolved in titanium as α or β stabiliser. In Ti6Al4V, Al (6%) acts as α stabiliser and V (4%) as β stabiliser. During the SLM process, due to the short laser-powder interaction, the localised heat input will lead to steep thermal gradients, rapid solidification and fast cooling (Vrancken et al., 2012). After solidification, acicular α' phase precipitated from prior β columnar grains was witnessed. During this quenching, as the temperature reaches 500 °C, precipitation of a Ti_3Al phase is possible since the solubility of Al in Ti is very low at this temperature. On re-melting the previously scanned layer, the material will remain at a high temperature for a long time leading to further precipitation. Precipitation of Ti_3Al has been previously witnessed for SLM fabricated parts (Lütjering, 1998). Hence the surface of the skin scanned/re-melted surface was observed to be richer in aluminium than the as-fabricated surface.

In the SLM process, as the material (Ti6Al4V) is melted by the laser, the constituent metals will react with the available interstitial elements (carbon, nitrogen and oxygen) in the build atmosphere (Ask et al., 1989). Although there is control over the oxygen level in the build chamber (less than 50 ppm) due to the explosive nature of the material, there will still be traces available for reaction. Also, the Ti6Al4V powder will itself contain oxygen. Hence, there is a

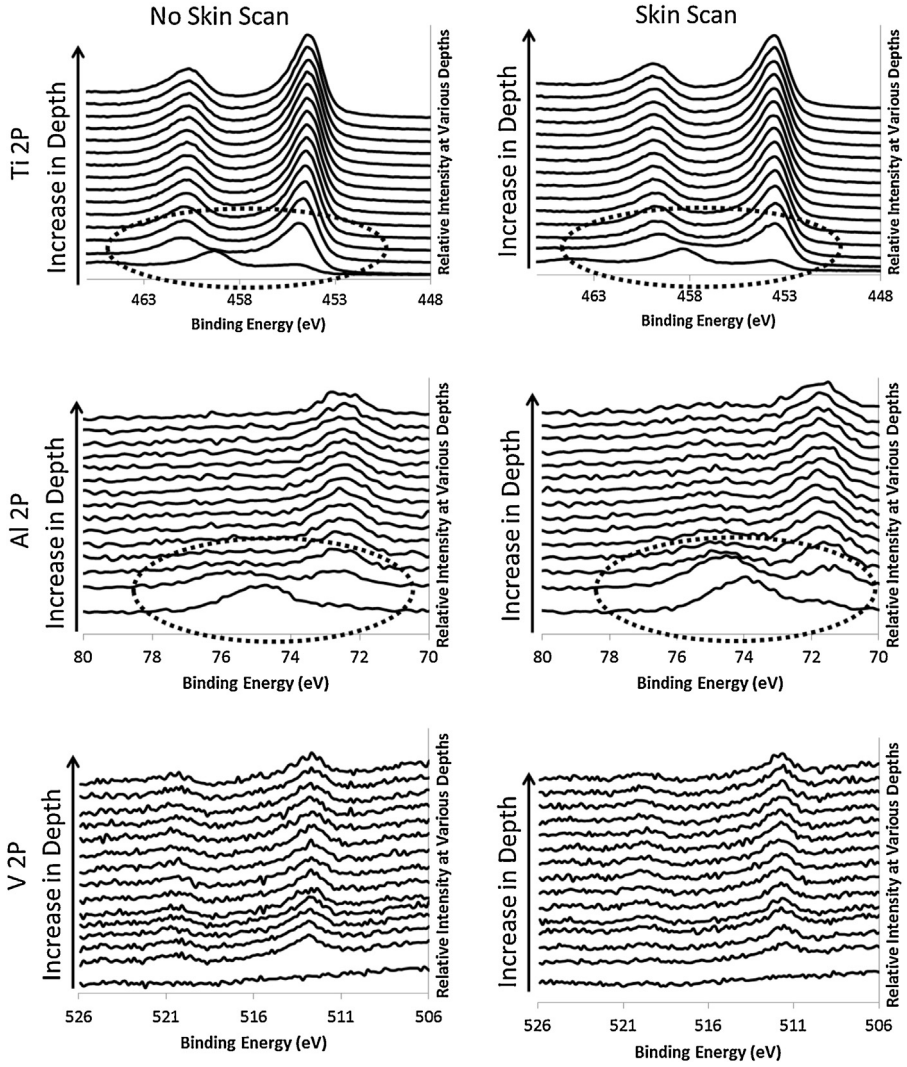

Fig. 4. XPS spectra of Ti 2p, Al 2p and V 2p regions for the non-skin scanned (NSK) and skin scanned (SK) Ti6Al4V surfaces fabricated by SLM. The dotted circles show the transformation of metal oxides to metals for Ti and Al.

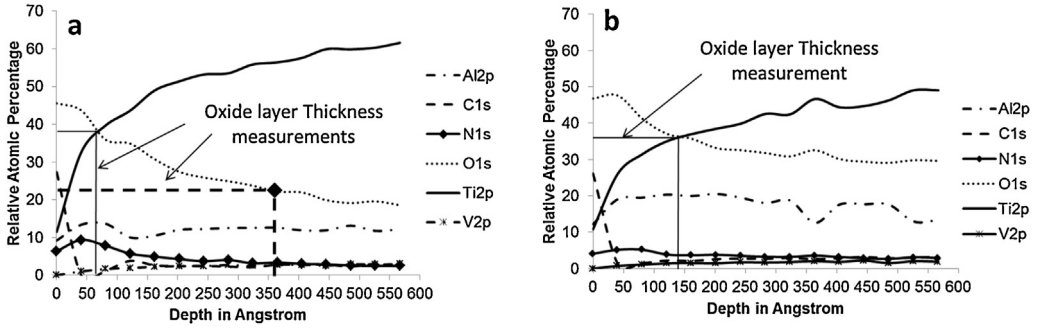

Fig. 5. Evolution of the surface composition of non-skin scanned (a) and Skin scanned (b) SLM fabricated surfaces.

high possibility for elements including Ti, Al and V to react with the available carbon, oxygen and nitrogen and form their corresponding carbides, oxides and nitrides. Fig. 3 exhibited the presence of carbides (282 eV) and nitrides (396.5 ± 0.2 eV) for both NSK and SK surfaces. The AM 250 has a built-in sensor to quantify the amount of oxygen in the chamber; but not for C and N. Also, C and N are present in the atmosphere as organic contaminants and as gases (CO, CO_2 and N_2). Due to the high reactivity of Ti and Al towards carbon and nitrogen these metal carbides and nitrides are formed (Ask et al., 1989). In addition to the formation of oxides of the metals and other interstitial elements, it should also be noted that oxygen is an α stabiliser and its presence could raise the transition temperature of the $\alpha + \beta$ alloy. Thus presence of oxygen in the build chamber can affect the SLM process and the surface chemistry of the fabricated part.

On studying the surface oxide film composition, both the NSK and SK surfaces mainly consisted of oxides of Ti and Al. However, their concentrations were significantly different. The NSK surface

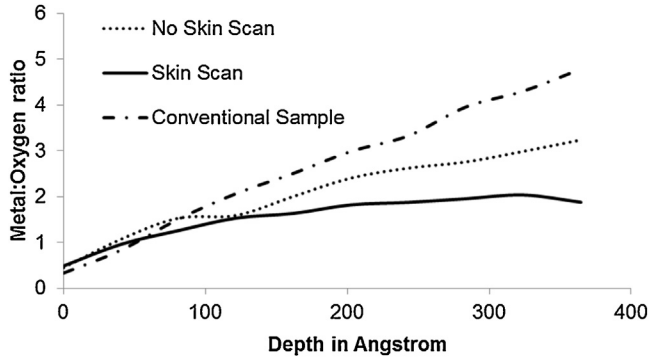

Fig. 6. A comparison of the oxide depth profile for the NSK, SK and CF Ti6Al4V samples.

rendered a surface oxide film rich in titanium whereas the SK surface rendered an oxide film rich in aluminium. Also the determined thickness of the oxide film was higher for the SK surface compared to the NSK surface. The main reason for the formation of a thick oxide layer on the SK surface is due to remelting or skin scanning. During SK, as the surface was melted twice, there was a high possibility for the penetration of oxygen from the build atmosphere further into the surface, thus leading to the formation of a thick oxide layer. Also, due to SK, there was a high possibility for the precipitation of Al (due to rapid heating and cooling cycles) on the surface, thus leading to an increased aluminium concentration on the SK surface. Fig. 6 clearly depicts the rate of decrease of oxide with depth to be in the order of CF > NSK > SK. One of the major reasons for the more gradual transition of the metal oxides to metal in NSK and SK surfaces is due to the formation of thick surface oxide layer. Also, when the NSK surface was remelted, a further reduction in oxide thickness can witnessed. This clearly indicated that SLM processing of Ti6Al4V is the major reason for producing a thicker surface oxide layer than the CF sample; however, surface remelting further increases the oxide layer thickness. It should be noted that on remelting, the laser scan tracks might have slightly increased the roughness of the SK surface and since XPS is highly sensitive to rough surfaces, there is the possibility for the results to be affected by this to a small level (Gunter et al., 1997; Martín-Concepción et al., 2004).

Ti6Al4V alloy is preferred for various applications because of the surface TiO_2 film. For automotive applications, the presence of this passive TiO_2 film offers high corrosion resistance. In biomedical applications, the presence of corrosion resistant TiO_2 film offers high biocompatibility. Also, SLM is considered as one of the viable processes to make customised metallic parts with complex structures. The use of SLM to fabricate such intricate parts will be limited if the process affects the surface chemical composition. Surface chemistry plays a pivotal role in determining the surface properties of a material (Mani et al., 2007). Small changes in the chemical composition may cause catastrophic loss of ductility and corrosion resistance (Manivasagam et al., 2010). Corrosion resistance is dependent on the surface oxide layer thickness. In general, the thicker the oxide layer is, the higher is the corrosion resistance. Surface oxide layers act as a barrier and prevent the release of metal ions from the bulk material. The corrosion resistance of the SLM fabricated Ti6Al4V has been discussed in literature (Chang and Lee, 2002). Vandenbroucke and Kruth (2007) reported that the corrosion resistance offered by the SLM fabricated Ti6Al4V parts satisfied the requirements for medical application. However, long-term use of Ti6Al4V implants for medical applications were observed to produce cytotoxic effects due to the release of Al and V ions (Elias et al., 2008). Since the SLM fabricated parts in this study produced surfaces with a higher concentration of aluminium than the bulk material, it is crucial to understand how the process conditions might affect the surface properties. Dai et al. (2015) reported that the existence of relatively large amounts of acicular α′-Ti phase compared to the β-Ti phase in an SLM sample as a main reason for poor corrosion resistance. The present study also observed a higher concentration of Al, the α stabilizer on the surface. This suggests that the presence of high concentration of Al on the surface will affect the corrosion resistance of SLM fabricated Ti6Al4V.

In addition to improving the surface quality, surface-remelting is also performed to improve the density of a fabricated part (Yasa and Kruth, 2011). This is achieved by remelting the previously laser-scanned layer to form an even surface. When the surface is even, the distribution of powder to build the next layer will be more homogenous and will reduce the entrapment of air. Hence, there is a high possibility to reduce pores and improve the density of the part. However, changes in the surface oxide composition may alter the wettability and could possibly result in balling phenomena (splitting-up of melt pool into tiny spheres/entities) and delamination of successive layers. Also precipitation of aluminium due to the impact of laser power may also affect the mechanical properties of SLM fabricated Ti6Al4V components. Thus where a strict control of the surface chemistry is required, the processing parameters must be chosen appropriately.

5. Conclusions

- The surface chemistry of the SLM fabricated NSK and SK surfaces were significantly different to the conventionally forged surface.
- Selective remelting/skin scanning of the final layer may be advantageous in terms of rendering an improved surface finish. However, it should be noted that it alters the surface chemical composition and the surface oxide layer.
- The surface oxide film of the skin scanned surface was enriched with oxides of aluminium whereas the surface oxide film of non-skin scanned surface was enriched with oxides of titanium. Also the concentration of vanadium on the skin scanned surface increased compared to the non-skin scanned surface.
- Since selective remelting alters the surface chemical composition by increasing aluminium and vanadium concentration on the surface, corrosion resistance and biocompatibility of these components may be significantly reduced.
- Further studies on the oxide layer thickness and corrosion resistance of the selective remelted and non-remelted parts would be beneficial to enable improved understanding.

Acknowledgement

This work was supported by the Engineering and Physical Sciences Research Council(EPSRC; UK) under grant EP/I033335/2.

References

Alrbaey, K., Wimpenny, D., Tosi, R., Manning, W., Moroz, A., 2014. J. Mater. Eng. Perform. 23, 2139–2148.
Aronsson, B.O., Lausmaa, J., Kasemo, B., 1997. J. Biomed. Mater. Res. 35, 49–73.
Ask, M., Lausmaa, J., Kasemo, B., 1989. Appl. Surf. Sci. 35, 283–301.
Biesinger, M.C., Lau, L.W.M., Gerson, A.R., Smart, R.S.C., 2010. Appl. Surf. Sci. 257, 887–898.
Chang, E., Lee, T.M., 2002. Biomaterials 23, 2917–2925.
Dai, N., Zhang, L.-C., Zhang, J., Chen, Q., Wu, M., 2015. Corros. Sci., 4–9.
Dementjev, A.P., Graaf, A., De Sanden Van De, M.C.M., Maslakov, K.I., 2000. Diamond Relat. Mater. 9, 1904–1907.
Elias, C.N., Lima, J.H.C., Valiev, R., Meyers, M., 2008. J. Miner. Met. Mater. Soc., 46–49.
Gibson, I., Rosen, D.W., Stucker, B., 2010. Additive Manufacturing Technologies. Springer, US, Boston, MA.
Gunter, P.L., Gijzeman, O.L., Niemantsverdriet, J., 1997. Appl. Surf. Sci. 115, 342–346.

Kruth, J., Badrossamay, M., Yasa, E., Deckers, J., Thijs L., Van Humbeeck, J., 2010. Part and material properties in selective laser melting of metals in: 16th International Symposium on Electromachining, 1–12.
Lütjering, G., 1998. Mater. Sci. Eng. A 243, 32–45.
Mani, G., Feldman, M.D., Patel, D., Agrawal, C.M., 2007. Biomaterials 28, 1689–1710.
Manivasagam, G., Dhinasekaran, D., Rajamanickam, A., 2010. Recent Patents Corros. Sci. 2, 40–54.
Martín-Concepción, I., Yubero, F., Espinós, J.P., Tougaard, S., 2004. Surf. Interface Anal. 36, 788–792.
Meier, H., Haberland, C., 2008. Materwiss. Werksttech. 39, 665–670.
Vaithilingam, J., Kilsby, S., Goodridge, R.D., Christie, S.D.R., Edmondson, S., Hague, R.J.M., 2014. Appl. Surf. Sci. 314, 642–654.
Vaithilingam, J., Kilsby, S., Goodridge, R.D., Christie, S.D.R., Edmondson, S., Hague, R.J.M., 2015. Mater. Sci. Eng. C 46, 52–61.
Vandenbroucke, B., Kruth, J.-P., 2007. Rapid Prototyp. J. 13, 196–203.
Variola, F., Yi, J.-H., Richert, L., Wuest, J.D., Rosei, F., Nanci, A., 2008. Biomaterials 29, 1285–1298.
Vrancken, B., Thijs, L., Kruth, J.-P., Van Humbeeck, J., 2012. J. Alloys Compd. 541, 177–185.
Warnke, P.H., Douglas, T., Wollny, P., Sherry, E., Steiner, M., Galonska, S., Sivananthan, S., 2009. Tissue Eng. Part C 15, 115–124.
Yadroitsev, I., Smurov, I., 2011. Phys. Procedia 12, 264–270.
Yasa, E., Kruth, J., 2011. Adv. Prod. Eng. Manag. 6, 259–270.